$ZnFe_2O_4$-C/$LiFePO_4$-CNT: A Novel High-Power Lithium-Ion Battery with Excellent Cycling Performance

*Alberto Varzi, Dominic Bresser, Jan von Zamory, Franziska Müller, and Stefano Passerini**

An innovative and environmentally friendly battery chemistry is proposed for high power applications. A carbon-coated $ZnFe_2O_4$ nanoparticle-based anode and a $LiFePO_4$-multiwalled carbon nanotube-based cathode, both aqueous processed with Na-carboxymethyl cellulose, are combined, for the first time, in a Li-ion full cell with exceptional electrochemical performance. Such novel battery shows remarkable rate capabilities, delivering 50% of its nominal capacity at currents corresponding to ≈20C (with respect to the limiting cathode). Furthermore, the pre-lithiation of the negative electrode offers the possibility of tuning the cell potential and, therefore, achieving remarkable gravimetric energy and power density values of 202 Wh kg^{-1} and 3.72 W kg^{-1}, respectively, in addition to grant a lithium reservoir. The high reversibility of the system enables sustaining more than 10 000 cycles at elevated C-rates (≈10C with respect to the $LiFePO_4$ cathode), while retaining up to 85% of its initial capacity.

1. Introduction

The lithium-ion battery market is growing beyond expectations. The continuous progresses achieved by the development of new and/or enhanced materials has led to considerable improvements in terms of both energy and power densities.[1] This has enabled, apart from the nowadays-established consumer electronics, further applications for lithium-ion batteries as, for instance, in the automotive sector (i.e., electric or hybrid vehicles). Nevertheless, there is still much room for improvement, especially concerning the high power density demanded by such kind of applications.

Since the diffusion of Li ions in and out of the electrode structure is frequently the rate determining step, this must be improved to allow a fast charge and discharge of the battery.[2] With this goal in mind, scientists have put substantial efforts on developing new nanostructured materials, which facilitate the Li ion diffusion due to a reduced diffusion length within the active material particles and an increased electrode/electrolyte contact area. A variety of both anode and cathode materials was proposed in form of nanoparticles, nanofibers, nanotubes, etc.[3] Additionally, highly structured carbon nanocomposites were developed to enhance not only the ionic but also the electronic conductivity of the electrode.[4] On the cathode side, carbon-coated $LiFePO_4$,[5] $LiMn_2O_4$,[6] and their composites with graphene[7] or carbon nanotubes[8–11] are, so far, the best candidates for use in high power devices. In regard to the negative electrode, Sn-C,[12,13] electrodeposited Fe_3O_4 on a nanostructured Cu current collector,[14] mesoporous Co_3O_4 nanowires,[15] and nanocrystalline $Li_4Ti_5O_{12}$ on carbon nanofibers[16] are some examples of innovative materials with very promising high rate performances.

While the scientific literature abounds in studies focusing on the performance of newly developed active materials in half-cell configuration, there are only very few reports on full batteries with power-oriented performance. Basically, the most common battery configurations are $Li_4Ti_5O_{12}$/$LiCoO_2$[17] and $Li_4Ti_5O_{12}$/$LiFePO_4$.[18] The latter system, when activated carbon is added to the positive electrode, was at the same time also investigated regarding its utilization as a lithium-ion capacitor.[19] However, the vast majority of these anyway only few studies utilized $Li_4Ti_5O_{12}$ as active material on the anode side. As an alternative, Derrien et al.[20] and Brutti et al.[21] recently reported very interesting results by combining a Sn-C-based anode with $LiNi_{0.5}Mn_{1.5}O_4$ and carbon-coated $LiFePO_4$ as cathode, respectively. Substituted metal oxides, such as the spinel $ZnCo_2O_4$ (e.g., 3D nanowire arrays on carbon cloth), were also demonstrated to be superior to graphite in terms of rate performance in flexible lithium-ion cells with $LiCoO_2$ cathodes.[22] Similar to $ZnCo_2O_4$, which combines conversion and alloying mechanism for the reversible lithium storage, $ZnFe_2O_4$ was also proposed as high capacity anode,[23–27] offering the great advantage of being more environmentally friendly, more cost-efficient, and less toxic due to the replacement of cobalt by iron. Bresser et al.[28] demonstrated very recently that, beside the reversible capacity values exceeding 1000 mA g^{-1}, carbon-coated $ZnFe_2O_4$

Dr. A. Varzi, D. Bresser, J. von Zamory, F. Müller, Prof. S. Passerini
Institute of Physical Chemistry & MEET Battery Research Center
University of Muenster
Corrensstrasse 28/30 & 46, 48149, Münster, Germany
E-mail: stefano.passerini@uni-muenster.de
Prof. S. Passerini
Helmholtz Institute Ulm
Albert Einstein Allee 11, 89097, Ulm, Germany

DOI: 10.1002/aenm.201400054

nanoparticles exhibit also excellent rate capability. Nevertheless, within their study they focused on the characterization of this new active material using half-cells only.

Here, we propose for the first time a novel battery configuration wherein carbon-coated $ZnFe_2O_4$ nanoparticles are employed as negative electrode material and a multiwalled carbon nanotube (CNT)-$LiFePO_4$ composite is used on the positive electrode side (also referred to here as $ZnFe_2O_4$-C/$LiFePO_4$-CNT). As a proof of concept, we demonstrate the great potential of such combination. In addition to the fact that only electrodes were employed, which were prepared using environmentally friendly, water-based Na-carboxymethyl cellulose as binder, more remarkably, this new lithium-ion full-cell provides advanced high rate performance and excellent cycling stability.

2. Results and Discussion

2.1. Characterization of $LiFePO_4$-CNT Cathode

Due to their rather poor electronic and ionic conductivities, cathode materials are frequently limiting the high power performance of lithium-ion batteries. Therefore, in order to keep up with the excellent rate capability of $ZnFe_2O_4$-C anodes (ZFO), carbon-rich $LiFePO_4$ (LFP) positive electrodes were prepared. Accordingly, commercial, carbon-coated, sub-micrometric LFP particles were embedded in an extensive network of multiwalled carbon nanotubes to form a composite cathode, which is hereinafter called LFP-CNT. As shown in **Figure 1**a, because of their tubular shape, CNTs form an extended electronically conductive network interconnecting the single LFP particles (see inset Figure 1a), thus guaranteeing an efficient and rapid electron transport. In fact, such a large amount of conductive additive most probably exceeds the electronic percolation threshold. Additionally, the excess of carbon nanotubes shall ensure an advanced high rate performance of the commercial LFP particles with respect to the targeted application in a high power lithium-ion full-cell. In fact, as suggested by Sotowa et al.[29] creating sufficient space between the particles CNT facilitate the electrolyte permeability, hence, decreasing the concentration polarization when the electrode is subjected to high current loads. As displayed in Figure 1b, the LFP-CNT positive electrode has a practical reversible capacity of 158 mAh g^{-1}_{LFP} at C/5. When the applied C rate is increased to 10C and 20C, such electrodes still provide specific capacities of 90 and 60 mAh g^{-1}_{LFP}, respectively. Considering the initial capacity, such values account for a capacity retention of ≈56% and 38%. Besides, except for the first cycle, for which an irreversible capacity of 27 mAh g^{-1} is observed, the coulombic efficiency of these LFP-CNT electrodes subjected to galvanostatic charge/discharge is very high, reaching values of almost 100% at C rates as high as 10C and 20C.

2.2. Pre-Formation of the $ZnFe_2O_4$-C Anode in Half-Cell Configuration

The detailed electrochemical characterization of the herein utilized ZFO-based anodes was already reported previously.[28] Such electrodes showed a remarkable rate performance and

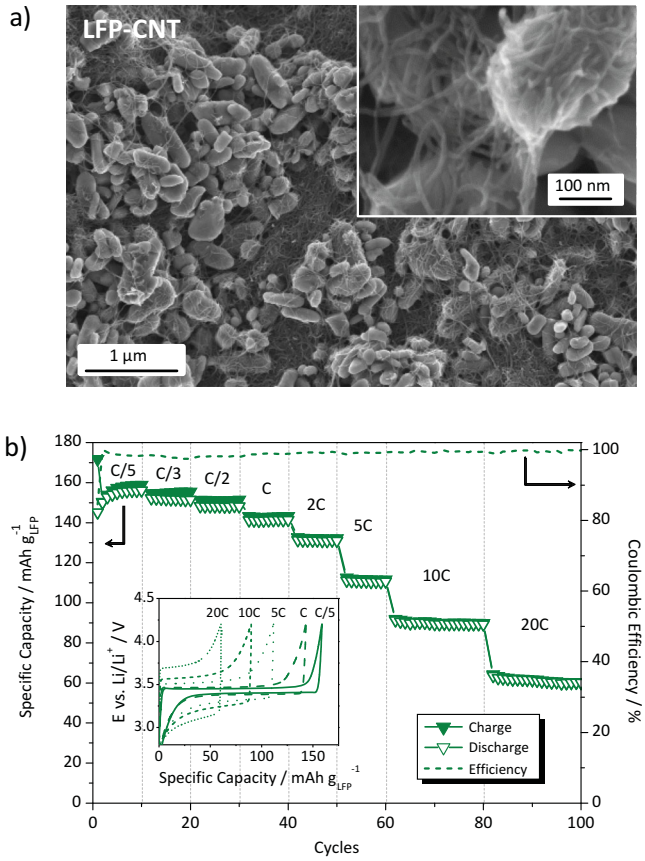

Figure 1. a) Scanning electron microscopy (SEM) images of LFP-CNT positive electrodes. Inset: the connection network established by CNT between the $LiFePO_4$ particles. b) Rate capability and coulombic efficiency of LFP-CNT cathodes (in half-cell configuration vs. Li) at C rates ranging from C/5 to 20C. Inset: some selected potential profiles at different current loads.

cycling stability. Being specifically interesting for the application of these electrodes in a lithium-ion full-cell, however, the irreversible charge consumption within the first cycle was slightly less than 30%. This initial irreversible capacity was mainly attributed to the formation of a solid electrolyte interphase (SEI) layer on the active material particles surface. Nevertheless, with respect to the anyway limited amount of lithium within a full-cell, the negative electrodes were electrochemically pre-lithiated prior to their assembly in the $ZnFe_2O_4$-C/$LiFePO_4$-CNT lithium-ion full-cells. This pre-lithiation was done by galvanostatic cycling the ZFO anodes in Li half-cells at relatively low current (C/10, i.e., ≈0.1 A g^{-1}). As displayed in **Figure 2**, after a slight increase during the initial cycles, ZFO anodes reach a stable reversible capacity of 1073 mAh g^{-1} at the 20th cycle. ZFO evenly provides capacity in the potential range from 0 to 2 V vs. Li/Li^+. However, it would be desirable to have a negative electrode mainly operating at rather low potentials in order to provide a higher energy density of the final lithium-ion full-cell. This is particularly true when LFP is used as cathode active material, which itself has a relatively low operating potential. Therefore, within the pre-lithiation step, anodes with three different lithiation degrees were prepared as shown in the inset in Figure 2. Accordingly, within thus processed electrodes a

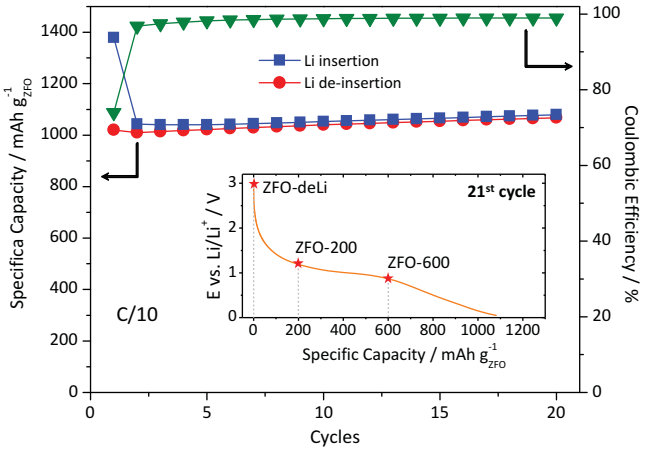

Figure 2. Electrochemical pre-lithiation of ZFO-based anodes in half-cell configuration (vs. Li). The inset shows the different degree of lithiation reached during the last reduction cycle.

specific capacity of 0 mAh g^{-1} (ZFO-deLi), 200 mAh g^{-1} (ZFO-200), and 600 (ZFO-600) mAh g^{-1} remained. These two levels of doping have been chosen to investigate the effect of the anode Li storage mechanism on the full cell performance. Indeed, doping the negative electrode with 200 mAh g^{-1} or 600 mAh g^{-1} allows to preferentially exploit the conversion mechanism or the alloying mechanism, respectively. The doping of the negative electrodes has, besides the tailoring of the full cell potential, the further function of introducing a Li reservoir into the system, which might buffer eventual irreversible charge consumption processes.

2.3. Lithium-Ion Full-Cells: $ZnFe_2O_4$-C/$LiFePO_4$-CNT

Here, different types of ZFO/LFP-CNT lithium-ion cells are presented with an average ZFO/LFP active mass ratio of 0.67. Despite the oversized cathode, the substantially lower specific capacity of LFP results in a positive to negative capacity ratio of ≈0.22 (calculated according to the practical capacities of the two active materials, i.e., about 160 mAh g^{-1} for LFP, obtained at the 10th cycle at C/5; and 1070 mAh g^{-1} for ZFO, obtained at the 20th cycle at C/10). Hence, the LFP-CNT cathodes in principle limit the capacity of all cells. Overall, three kinds of full-cells were assembled with fresh LFP-CNT cathodes and pre-formed ZFO anodes. With respect to the lithiation degree of the negative electrode, the cells are labeled as follows: "ZFO-deLi/LFP-CNT" (fully de-lithiated anode), "ZFO-200/LFP-CNT" (anode doped with 200 mAh g^{-1}) and "ZFO-600/LFP-CNT" (anode doped with 600 mAh g^{-1}). Although the doping leads to increased positive to negative capacity ratios (ZFO-200 and ZFO-600 have a practical capacity of ≈870 mAh g^{-1} and 470 mAh g^{-1}, respectively), this remains considerably lower than the unity (i.e., 0.28 and 0.51 for ZFO-200/LFP-CNT and ZFO-600/LFP-CNT, respectively) and, therefore, all devices are still cathode limited. The performances of this novel type of battery have been investigated by galvanostatic cycling with current densities ranging from 0.05 to 6 mA cm^{-2}. Given the different capacities and active material mass loadings of the individual electrodes, the current effectively applied to the cells are also reported in A g^{-1} and C-rate with respect to both anode and cathode (see **Table 1**).

Figure 3a displays the voltage profiles of the full-cells during the first charge/discharge cycles at a very low current (i.e., 0.1 mA cm^{-1}). As expected, the partial lithiation of the negative electrode has a clear influence on the shape of the curves, which, in the case of ZFO-200/LFP-CNT and ZFO-600/LFP-CNT, show the typical plateau of ZFO at 1 V (lithiation) and 1.5 V (de-lithiation) vs. Li/Li$^+$. The full-cell employing the ZFO-deLi anode displays a much steeper voltage profile instead. Besides, the aspect appearing most noteworthy is the influence of the negative electrode doping level on the average discharge voltage of the cell. While the ZFO-deLi/LFP-CNT cell has a relatively low cell voltage of 1.58 V, the ZFO-200 and ZFO-600 anodes operate in a more negative voltage range, thus enabling a considerable increase of the cell discharge potential up to 1.69 V and 2.12 V, respectively.

The capacity delivered by the full-cells under increasing current density is reported in Figure 3b. All devices display an initial capacity increase upon the first 20 cycles. Such behavior closely resembles the results observed in Figure 1b and, therefore, can be attributed to the initial activation of the LFP-CNT cathode. The capacity values obtained at the 20th cycle approach the practical capacity of the positive electrode, accounting for specific capacities ranging from 93 to 101 mAh g^{-1} depending on the active material mass loading of both electrodes. The different lithiation degree of the ZFO anodes does not appear to considerably affect the rate capability of the full-cells. All cells deliver more than 50% of the initial capacity for the highest applied current density of 6 mA cm^{-2}. It is worth to notice that such a current density corresponds to 4.89C and 19.23C for ZFO and LFP, respectively. Differently from the ZFO-200/LFP-CNT and ZFO-600/LFP-CNT cells, which show very stable capacity values at any current density, the ZFO-deLi/LFP-CNT cell seems to suffer of a certain capacity fading when the current density exceeds 0.5 mA cm^{-2}. At such current densities, as clearly noticeable from the voltage profiles displayed in Figure 3c, the ZFO-deLi anode becomes limiting during the cell discharge. In fact, due to the increasing polarization, the potential of the fully de-lithiated negative electrode easily reaches the upper cut-off potential (i.e., 2.8 V vs. Li/Li$^+$, equivalent to the LFP-CNT lower cut-off), leading to the incomplete utilization of the positive electrode and, subsequently, to a progressive

Table 1. Conversion between current densities applied to the full-cells and the respective values given as C rate and A g^{-1} related to both the anode (ZFO) and cathode (LFP) active material.

Current applied to the full-cell [mA cm^{-2}]	ZFO (C_{th}: 1000 mAh g^{-1})		LFP (C_{th}: 170 mAh g^{-1})	
	[A g^{-1}]	[C]	[A g^{-1}]	[C]
0.1	0.08	0.08	0.05	0.32
0.5	0.41	0.41	0.27	1.59
1	0.82	0.82	0.54	3.19
2	1.63	1.63	1.09	6.41
3	2.45	2.45	1.63	9.61
6	4.89	4.89	3.26	19.23

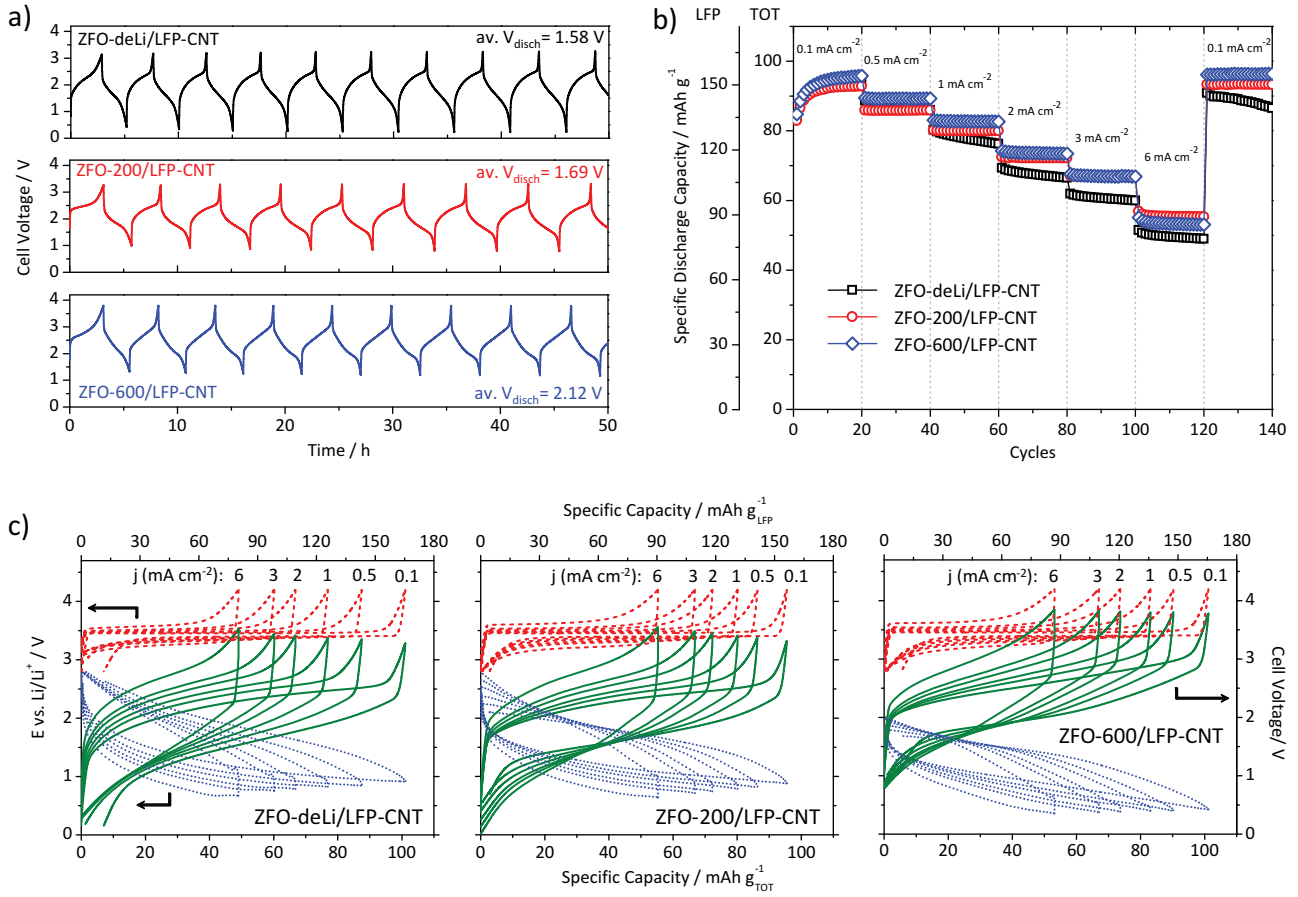

Figure 3. Electrochemical performance of ZFO/LFP-CNT full-cells employing ZFO anodes with different degrees of lithiation. a) Cell voltage profiles for such cells upon galvanostatic cycling at 0.1 mA cm^{-2} and influence of the lithiation degree on the average discharge voltage. b) Rate capability as function of the applied current density (from 0.1 to 6 mA cm^{-2}) and c) relative voltage profiles of the individual electrodes and their influence on the overall cell voltage curves. Specific discharge capacity values are referred to the active material amount of both the limiting cathode (i.e., LFP) and the overall cell (i.e., TOT = LFP+ZFO).

capacity fading at elevated rates. This phenomenon is not observed in ZFO-200/LFP-CNT and ZFO-600/LFP-CNT cells for which the anodes, because of the introduction of a defined amount of Li, operates in a more negative voltage window, thus buffering the voltage increase caused by polarization. In **Figure 4**a, the average discharge voltage of the investigated cells is plotted as a function of the applied current density. Up to 1 mA cm^{-2} the doping turns out to be a generally effective strategy for raising the full-cell discharge potential. However, in the case of the ZFO-200/LFP-CNT cell, when the load is increased, the average voltage drops to values comparable (and even lower) to those of the ZFO-deLi/LFP-CNT cell.

Although it might appear surprising, this is a direct consequence of the previously mentioned incomplete utilization of the cathode material in the ZFO-deLi/LFP-CNT cell caused by the limiting anode during discharge. As a matter of fact, the positive electrode voltage does not approach its lower limit during the cell discharge (see left plot in Figure 3c). This corresponds to a higher average cell voltage, but lower capacity. For the cell containing the ZFO-200 negative electrode, both electrodes are approaching their full discharge (center plot of Figure 3c) and thus the LFP-CNT electrode voltage is steeply decreasing toward the end of the discharge. This means that the average voltage of the LFP electrode is lower than in the previous cell, which results in a lower average cell voltage. The cell capacity, however, is higher.

Differently, the discharge voltage of the ZFO-600/LFP-CNT cell is remarkably retained upon increasing the current density because of the large amount of lithium stored in ZFO-600, resulting in a lower average anode voltage. Even for the maximum applied current density of 6 mA cm^{-2}, it is 0.43 V higher than that of the ZFO-deLi/LFP-CNT cell. Such phenomenon would suggest faster kinetics of the alloying mechanism compared to the conversion mechanism. As clearly shown by the Ragone-like plot, displayed in Figure 4b, the substantially higher cell voltage results in a remarkable improvement in terms of full-cell specific energy. In fact, while all cells display very high specific power, even exceeding 3 kW kg^{-1} (i.e., 3.02 kW kg^{-1} and 3.72 kW kg^{-1} at 6 mA cm^{-2} for ZFO-deLi/LFP-CNT and ZFO-600/LFP-CNT, respectively), only the ZFO-600/LFP-CNT has a considerably higher specific energy. Specifically, the doping with 600 mAh g^{-1} leads to a gain in specific energy of about 37–40% compared to the other two cells, independently from the applied current. The innovative

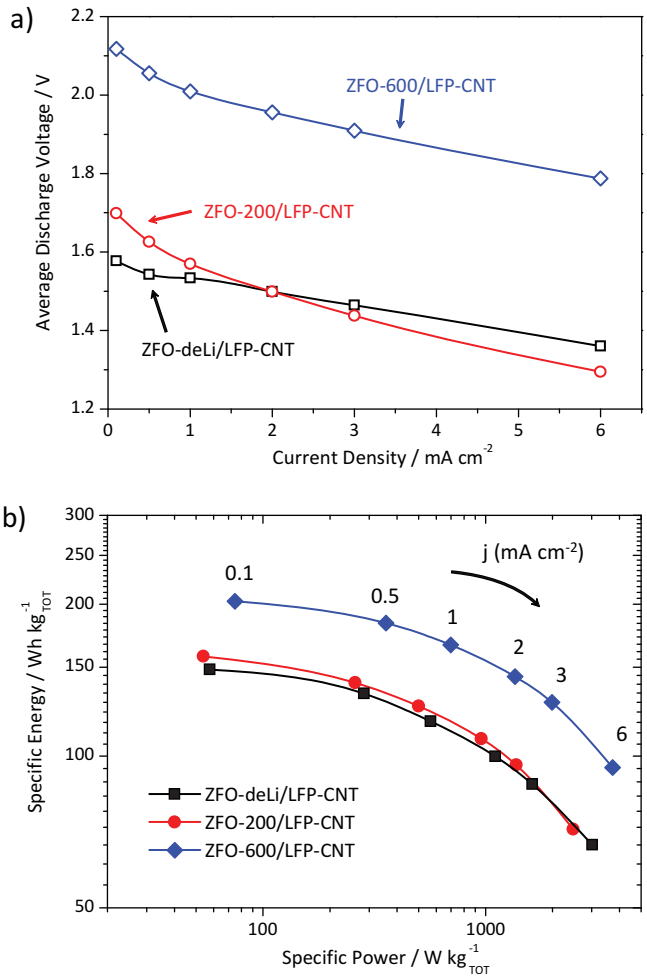

Figure 4. a) Effect of the current density on the average discharge voltage of ZFO/LFP-CNT cells and b) Ragone-like plot displaying their specific energy and power (referred to the total active material amount, i.e., LFP+ZFO).

combination ZFO/LFP-CNT we propose in this work demonstrates therefore incredibly promising features. This cell chemistry displays maximum power values similar to those of lithium-ion capacitors (LIC), while offering considerably higher specific energies. To the best of our knowledge, the highest specific energies reported for LIC have been achieved by graphite/AC systems and, referred to the weights of the active materials, barely exceed 100 Wh kg^{-1}.[30] So far, the highest value (125 Wh kg^{-1}) was obtained by Kim et al., using an artificial graphite anode,[31] which is considerably lower than the values provided by the ZFO/LFP-CNT cells. In fact, although we are aware that comparing specific energies obtained at different power/current is not fully appropriate, we do believe that the value of 202 Wh kg^{-1} (at 0.1 mA cm^{-2}) shown by the ZFO-600/LFP-CNT represents a remarkable achievement, testifying the great potential of such novel battery chemistry. The ZFO/LFP-CNT cells (as well as most lithium-ion capacitors) contain a not negligible amount of carbon and binder. However, the specific capacity values are still remarkable (see detailed values displayed in **Table 2**). Indeed, considering the total mass of

Table 2. Specific energy of ZFO/LFP-CNT cells obtained from galvanostatic discharge at 0.1 mA cm^{-2}. The values are calculated with respect to the active material (AM), active material and carbon (AM+C) and active material, carbon and binder (AM+C+B) weights of both electrodes.

Full cell	Specific Energy [Wh kg^{-1}]		
	AM	AM+C	AM+C+B
ZFO-deLi/LFP-CNT	148	105	96
ZFO-200/LFP-CNT	158	112	103
ZFO-600/LFP-CNT	202	144	132

the electrodes (including active materials, carbon and binder), the ZFO-600/LFP-CNT cells deliver 132 Wh kg^{-1}. Such a value accounts for an improvement of almost 30% with respect to the 103.8 Wh kg^{-1} reported by Khomenko et al.[32]

A further key feature of the ZFO/LFP-CNT cells is their impressive cycling stability. In fact, as shown in **Figure 5**a, such cells are able to sustain 10 000 galvanostatic cycles at a current density of 3 mA cm^{-2} (i.e., 9.61C for LFP and 2.45C for ZFO) with rather limited capacity fading. After a few stabilization cycles, the cells deliver rather similar capacities comprised between 42 and 48 mAh g^{-1}_{TOT} (corresponding to 75–86 mAh g^{-1}_{LFP}) for the 10th discharge. In the following cycles, however, while for ZFO-deLi/LFP-CNT a rather rapid decrease in capacity after 1000 cycles is observed, the cells assembled with doped anodes display considerably stable capacity retentions. After 10,000 cycles, ZFO-200/LFP-CNT and ZFO-600/LFP-CNT still deliver specific capacities of respectively 33 and 41 mAh g^{-1}_{TOT} (i.e., 60 and 74 mAh g^{-1}_{LFP}). In regard to the initial capacities (considered at the 10th cycle) such values account for a capacity retention of 79% and 85% for ZFO-200/LFP-CNT and ZFO-600/LFP-CNT, respectively.

As expected, the capacity fading is generally accompanied by an increase in polarization between charge and discharge. From the selected voltage profiles displayed in Figure 5b it is evident that the ZFO anode is the primary cause of such increase. Structural changes in the active material, as well as passivation of the electrode surface might be responsible for this behavior. In any case, such processes seem to take place mainly upon the first 5000 cycles. While this applies strictly to ZFO-200/LFP-CNT and ZFO-600/LFP-CNT, the performance of the ZFO-deLi/LFP-CNT cell appears to be additionally affected by a continuous capacity loss of the positive electrode. Considering that the cathode is in this cell the only lithium source besides the electrolyte, it is reasonable to attribute such decay to the lithium depletion in LFP. This phenomenon is avoided (or at least significantly delayed) in the other two cells within which, due to the partial lithiation of the ZFO anodes, a Li reservoir was generated, which is able to buffer the irreversible charge consumption upon cycling. Apart from this, no particular ageing phenomenon appears to have a dramatic effect on the performance of ZFO/LFP-CNT cells. This finding is strongly supported by the impedance spectra displayed in **Figure 6**. Indeed, the Nyquist plots recorded after 10 000 cycles highly resemble those of the fresh cells. No additional semicircles or peculiar features are detected, although, of course, a certain increase of the overall

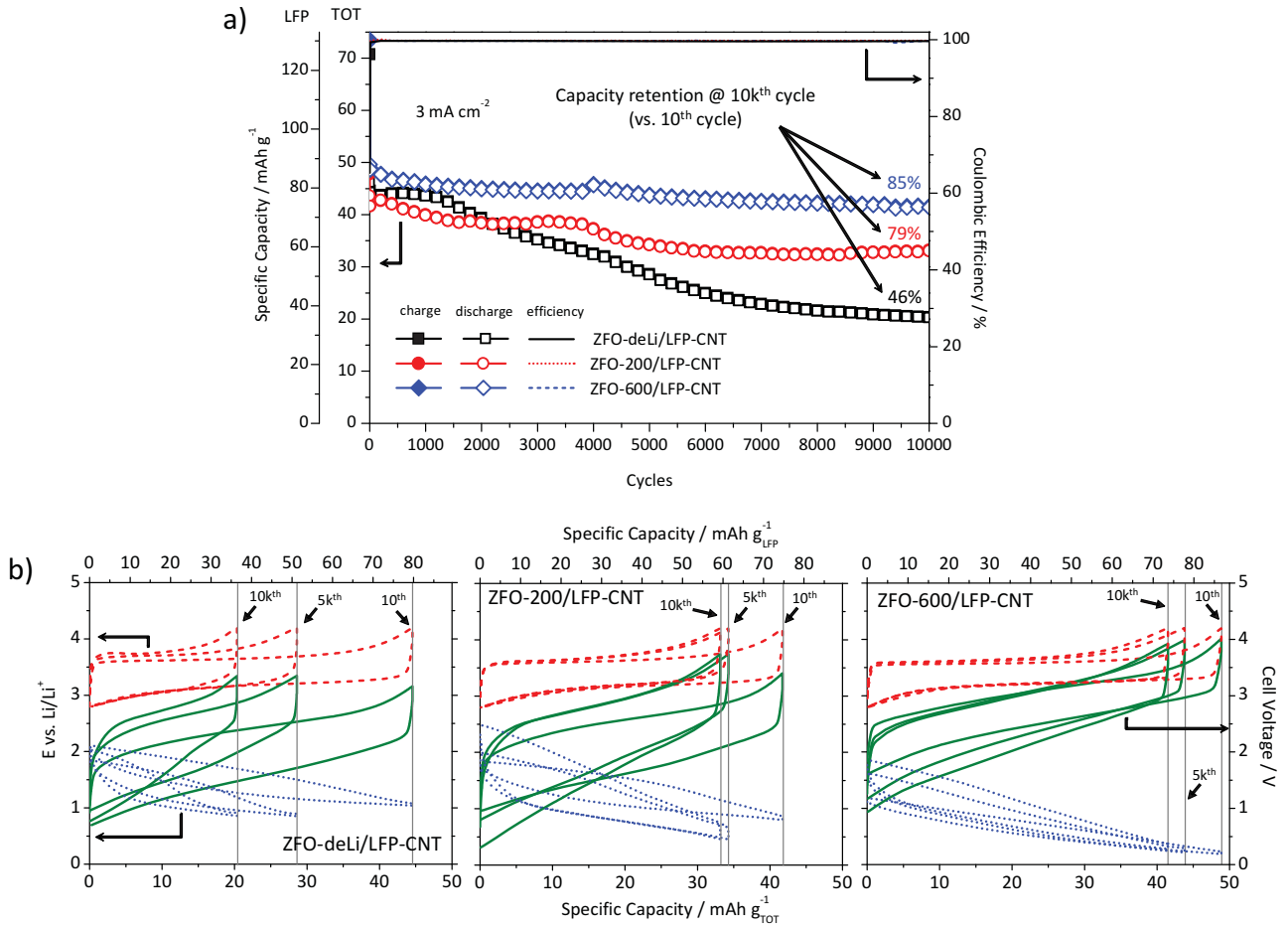

Figure 5. a) Long-term cycling stability applying a high current density of 3 mA cm^{-2} and the coulombic efficiency of ZFO/LFP-CNT full-cells employing anodes with different degrees of lithiation. b) Selected electrode and cell voltage profiles evolution upon cycling. Specific capacity values are referred to the active material amount of both the limiting cathode (i.e., LFP) and the sum of the anode and cathode (i.e., TOT = LFP+ZFO).

cell impedance is observed. As shown in Figure 6 insets, this is mostly due to: i) higher electrolyte resistance (identified by the high frequency intercept with the Z_{real} axis) and ii) contact/charge transfer resistance (evidenced by the diameter of the high frequency semicircle). However, such increases are, in our opinion, acceptable for cells operating for such a large number of cycles.

After recording the impedance spectra, the same full cells that underwent 10 000 cycles at 3 mA cm^{-2}, have been further cycled at low currents (see **Figure 7**). Upon 50 cycles at 0.5 mA cm^{-2} ZFO-deLi/LFP-CNT, ZFO-200/LFP-CNT, and ZFO-600/LFP-CNT showed stable capacities of 63, 62, and 68 mAh g^{-1}_{TOT}. In regard to the values obtained at the same current before the stability tests (see Figure 3b), these numbers results in remarkable capacity retentions of 73%, 72%, and 76% for ZFO-deLi/LFP-CNT, ZFO-200/LFP-CNT, and ZFO-600/LFP-CNT, respectively.

Finally, the effect of the electrochemical studies on the morphology of the ZFO anodes was investigated using SEM. SEM images of pristine and cycled electrodes (with different initial levels of Li doping) are displayed in **Figure 8**. At a first glance, no dramatic differences can be observed for pristine and cycled electrodes. This somehow confirms the previously mentioned (see Figure 6) absence of any particular ageing phenomenon. Nevertheless, a more detailed look reveals some peculiar features appearing on the electrodes cycled at high current rates for 10 000 cycles. As shown in Figure 8b, the prolonged operation of ZFO-deLi at potentials above 1 V vs. Li/Li^+ (resulting on a main storage of Li through the conversion mechanism) leads to the formation of large agglomerates, which may be responsible for the voltage profile shape change previously mentioned (see Figure 5b, left panel). As the anode working potential decreases (in-line with the remaining amount of lithium within the anode after the doping), these clusters become smaller (i.e., ZFO-200, see Figure 8c) and practically disappear in ZFO-600 (Figure 8d), for which the Li is presumably mostly stored via the alloying mechanism with Zn.

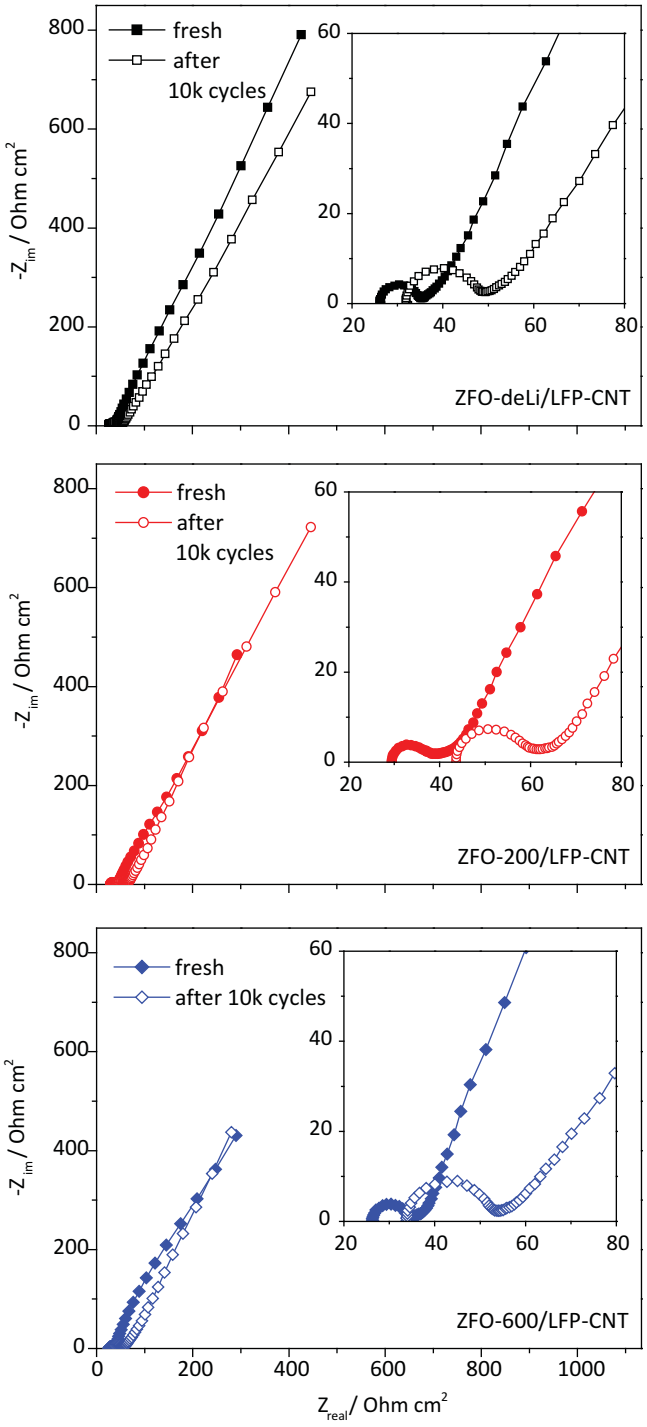

Figure 6. Impedance spectra of fresh and cycled ZFO/LFP-CNT full-cells. The insets show in detail the spectra in the medium-high frequency range.

3. Conclusions

In this work we proposed a novel battery configuration for high power applications. For the first time we have demonstrated, as a proof of concept, the highly promising features of lithium-ion full-cells combining carbon-coated $ZnFe_2O_4$ anodes and composite $LiFePO_4$-multi walled carbon nanotubes cathodes.

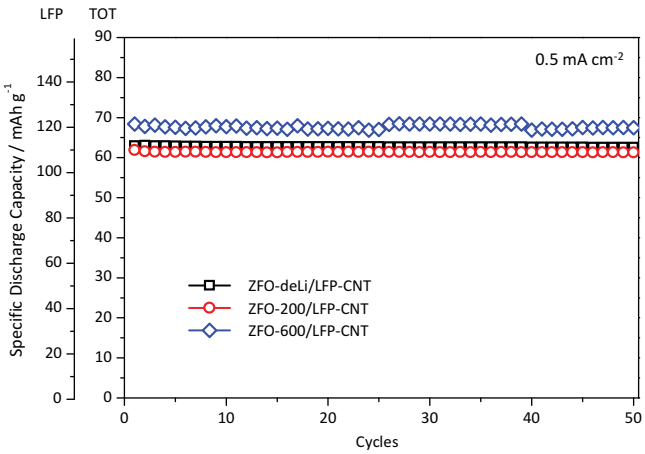

Figure 7. Galvanostatic cycling at 0.5 mA cm^{-2} after long cycling at high current. Specific capacity values are referred to the active material amount of both the limiting cathode (i.e., LFP) and the overall cell (i.e., TOT = LFP+ZFO).

ZFO/LFP-CNT cells showed remarkable rate capability retaining more than 50% of the initial capacity at C rates as high as ≈20C with respect to the limiting cathode. Moreover, a partial lithiation of the ZFO anode does not only enable an enhanced cycling stability of the full-cell, but does also result in an increased average full-cell discharge voltage while not substantially affecting the high rate performance. Among the investigated cells, the battery employing the negative electrode with the highest lithiation degree (600 mAh g^{-1}, i.e., ZFO-600/LFP-CNT) showed the best performance, delivering a maximum specific energy and power of 202 Wh kg^{-1} and 3.72 kW kg^{-1}, respectively (these values refer to the total active material amount of both electrodes). Due to the high reversibility of this system, such cells show a stable cycling performance at high current (3 mA cm^{-2}, i.e., ≈10C with respect to LFP), showing a capacity retention of 85% after 10 000 cycles. In addition, 76% of the initial capacity is recovered when cycled subsequently applying lower current densities of, e.g., 0.5 mA cm^{-2}. Beside the remarkable performance, a great advantage of this novel high power battery is represented by its environmental friendly nature. Zn and Fe are benign and highly abundant elements and both electrodes are produced via aqueous processing employing a cellulose-based binder.

4. Experimental Section

Electrode Preparation: Positive composite electrodes (labelled LFP-CNT) were prepared by processing all components in water. These were: carbon-coated $LiFePO_4$ (C_{th}: 170 mAh g^{-1}; LFP P2, Südchemie/Clariant, Germany), multiwalled carbon nanotubes (MWCNT Nanocyl-3101, Nanocyl, Belgium) and Na-carboxymethyl cellulose (CMC, Walocel CRT 2000PA, Dow Wolff Cellulosics, Germany), in the weight ratio 60:30:10. CMC was firstly dissolved in milli-Q deionized water to obtain a 1 wt% solution. Afterwards, MWCNT were added to the binder solution and, in order to promote their dispersion, such an aqueous mixture was treated in an ultrasonic bath for 2 h. Subsequently, LFP was added to the obtained homogeneous slurry, further stirred with a magnetic stirrer for 2 h, and then casted onto aluminium foil by the doctor blade technique (wet film thickness of 400 μm). Negative electrodes (labelled ZFO) were also processed in water by mixing

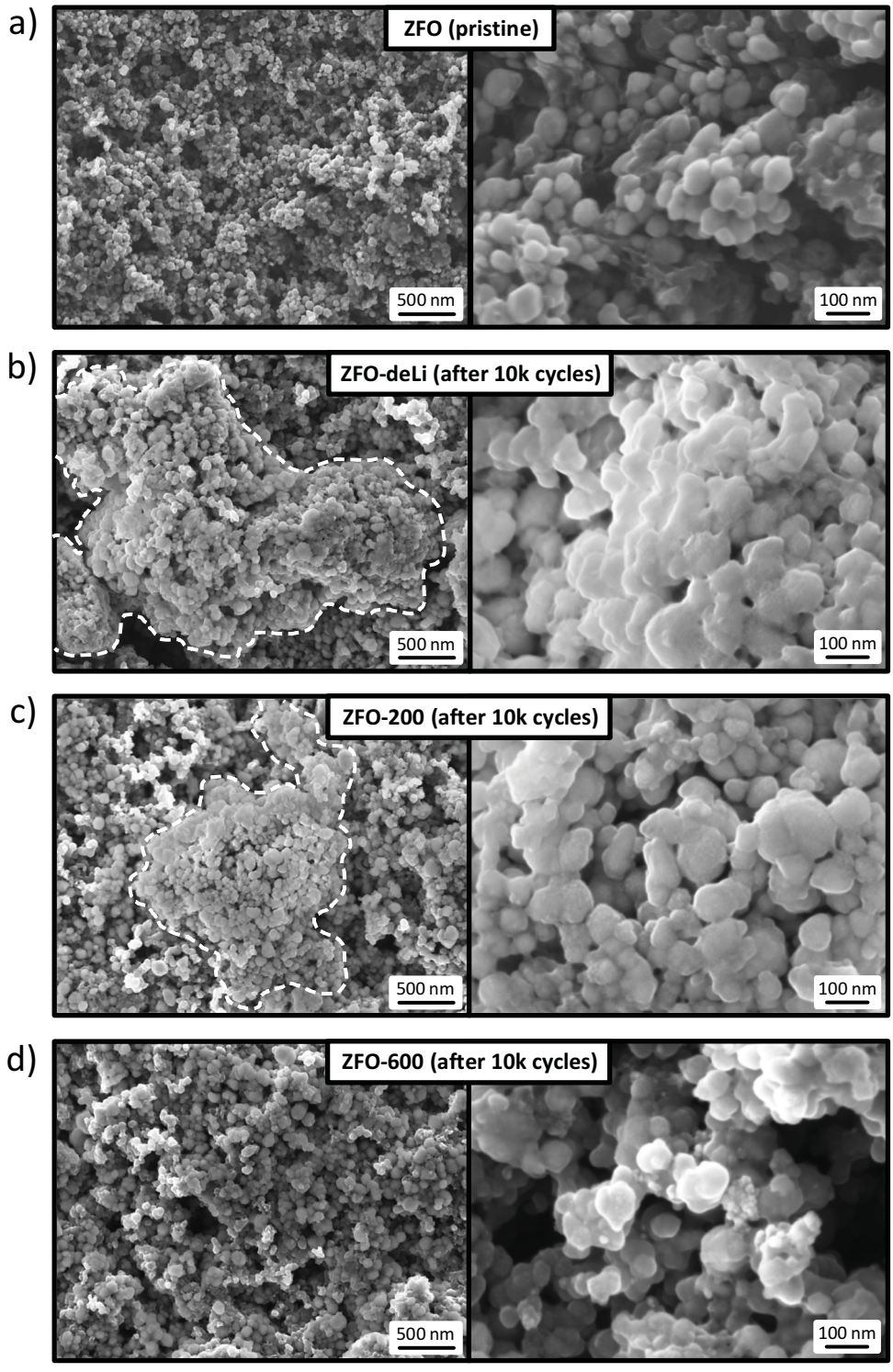

Figure 8. SEM images of ZFO anodes at different magnifications. Comparison between: a) pristine ZFO negative electrodes and b) ZFO-deLi, c) ZFO-200 and d) ZFO-600 electrodes after 10 000 cycles at 3 mA cm^{-2}. The white dashed lines highlight the regions more affected by the agglomeration of the ZFO nanoparticles.

carbon-coated $ZnFe_2O_4$ (a detailed description of the synthesis is given in ref. [28], C_{th} ≈1000 mAh g^{-1}), conductive carbon (Super C65, TIMCAL, Switzerland), and CMC in the weight ratio 75:20:5. The thus obtained mixture was ball milled for 2 h and the resulting slurry was then cast on dendritic copper foil (Schlenk, wet film thickness: 120 μm). The electrode sheets were firstly dried at room temperature and then transferred to an oven set at 80 °C for further drying overnight. Positive and negative electrodes (with a mass loading of ≈1.8 and 1.2 mg cm^{-2},

respectively) were then punched in disks (diameter: 12 mm) and dried for additional 12 h under vacuum at 180 °C prior to the electrochemical and morphological characterization.

Electrodes and Cells Characterization: The electrochemical measurements were carried out in three electrode Swagelok-type cells assembled in an Ar-filled glove box (MBraun, Germany; oxygen and water content < 0.1 ppm). Polypropylene fleeces (Freudenberg FS 2226) were used as separators and drenched with 100 µL of electrolyte (1 M $LiPF_6$ in ethylene carbonate (EC) and diethylcarbonate (DEC) mixed in a 3:7 volume ratio). Half-cells, comprising battery grade metallic Li (Rockwood Lithium, Germany) serving as counter and reference electrodes, were used for: i) preliminary investigations on the LFP-CNT cathode performance, and ii) the ZFO anodes pre-formation/doping. The detailed characterization of the negative electrodes in half-cell configuration was already reported in detail by Bresser et al.[28] LFP-CNT composite electrodes were characterized by galvanostatic cycling with potential limitation (2.8–4.2 V vs. Li/Li^+) at current rates ranging from C/5 to 20C (i.e., from 0.034 to 3.4 A g^{-1}). For the ZFO-based negative electrodes a pre-formation treatment in half-cells was performed, which was constituted of 20 galvanostatic cycles in the potential range 3–0.05 V vs. Li/Li^+ at C/10 (i.e., 0.1 A g^{-1}) and, for the partially lithiated ones, of a further reduction (21st cycle) limited to 200 mAh g^{-1} (ZFO-200) or 600 mAh g^{-1} (ZFO-600). Prior to their assembly in full-cells, the pre-formed anodes were disassembled in the glove box and rinsed with fresh electrolyte. In the full-cells, a reference electrode (metallic Li) was also employed for monitoring the individual electrode potentials. Upon galvanostatic cycling the operational potential windows for these were limited to 4.2–2.8 V vs. Li/Li^+ for the LFP-CNT cathode and 2.8–0.05 V vs. Li/Li^+ for the ZFO anode. Hence, the maximum cell voltage window allowed was 4.15 V. Rate capability tests were performed at current densities as high as 6 mA cm^{-2}, corresponding to almost 20C for LFP-CNT and 5C for ZFO. Impedance spectra of fresh and cycled (after 10 000 cycles) cells were collected under rest conditions (open circuit potential) in the frequency range comprised between 500 kHz and 10 mHz, with a sinusoidal amplitude of 5 mV. All electrochemical measurements were performed by means of a programmable multi-channel potentiostat-galvanostat (VMP3, Biologic Science Instruments) in a climatic chamber (KBF115, Binder GmbH) at 20 °C ± 2 °C. The morphology of both fresh and aged electrodes was also investigated by means of SEM. The cells containing the aged electrodes were disassembled in an Ar-filled glove box (MBraun), and the electrodes were carefully rinsed with dimethyl carbonate (DMC). In order to avoid contact with air and moisture, the samples have been transferred to the microscope using a homemade vacuum-sealed sample holder. Electrodes micrographs were acquired with a Carl Zeiss AURIGA Scanning Electron Microscope equipped with a field emission electron gun as electron source and an in-lens detector. The acceleration voltage was set to 3 kV.

Acknowledgements

The authors would like to acknowledge the University of Münster, the Bundesministerium für Bildung und Forschung (BMBF) within the project "IES, Innovative Elektrochemische Superkondensatoren" (contract number 03EK3010), and the European Commission within the "ORION" project (229036) under the Seventh Framework Programme (7th FWP) for the financial support.

Received: January 10, 2014
Revised: February 4, 2014
Published online: March 24, 2014

[1] J. M. Tarascon, M. Armand, *Nature* **2001**, *414*, 359.
[2] B. Scrosati, J. Garche, *J. Power Sources* **2010**, *195*, 2419.
[3] Y. Wang, G. Cao, *Adv. Mater.* **2008**, *20*, 2251.
[4] D. S. Su, R. Schlögl, *ChemSusChem* **2010**, *3*, 136.
[5] G. Xu, F. Li, Z. Tao, X. Wei, Y. Liu, X. Li, Z. Ren, G. Shen, G. Han, *J. Power Sources* **2014**, *246*, 696.
[6] E. Hosono, T. Kudo, I. Honma, H. Matsuda, H. Zhou, *Nano Lett.* **2009**, *9*, 1045.
[7] G. Kucinskis, G. Bajars, J. Kleperis, *J. Power Sources* **2013**, *240*, 66.
[8] L. Kavan, R. Bacsa, M. Tunckol, P. Serp, S. M. Zakeeruddin, F. Le Formal, M. Zukalova, M. Graetzel, *J. Power Sources* **2010**, *195*, 5360.
[9] A. Varzi, C. Täubert, M. Wohlfahrt-Mehrens, *Electrochim. Acta* **2012**, *78*, 17.
[10] G. Qin, Q. Wu, J. Zhao, Q. Ma, C. Wang, *J. Power Sources* **2014**, *248*, 588.
[11] X.-M. Liu, Z. D. Huang, S. W. Oh, B. Zhang, P.-C. Ma, M. M. F. Yuen, J.-K. Kim, *Compos. Sci. Technol.* **2012**, *72*, 121.
[12] J. Hassoun, G. Derrien, S. Panero, B. Scrosati, *Adv. Mater.* **2008**, *20*, 3169.
[13] D. Bresser, F. Mueller, D. Buchholz, E. Paillard, S. Passerini, *Electrochim. Acta* **2013**, DOI 10.1016/j.electacta.2013.09.007.
[14] P. L. Taberna, S. Mitra, P. Poizot, P. Simon, J.-M. Tarascon, *Nat. Mater.* **2006**, *5*, 567.
[15] Y. Li, B. Tan, Y. Wu, *Nano Lett.* **2008**, *8*, 265.
[16] K. Naoi, S. Ishimoto, Y. Isobe, S. Aoyagi, *J. Power Sources* **2010**, *195*, 6250.
[17] G. X. Wang, D. H. Bradhurst, S. X. Dou, H. K. Liu, *J. Power Sources* **1999**, *83*, 156.
[18] A. Jaiswal, C. R. Horne, O. Chang, W. Zhang, W. Kong, E. Wang, T. Chern, M. M. Doeff, *J. Electrochem. Soc.* **2009**, *156*, A1041.
[19] X. Hu, Y. Huai, Z. Lin, J. Suo, Z. Deng, *J. Electrochem. Soc.* **2007**, *154*, A1026.
[20] G. Derrien, J. Hassoun, S. Panero, B. Scrosati, *Adv. Mater.* **2007**, *19*, 2336.
[21] S. Brutti, J. Hassoun, B. Scrosati, C.-Y. Lin, H. Wu, H.-W. Hsieh, *J. Power Sources* **2012**, *217*, 72.
[22] B. Liu, J. Zhang, X. Wang, G. Chen, D. Chen, C. Zhou, G. Shen, *Nano Lett.* **2012**, *12*, 3005.
[23] Y.-N. NuLi, Y.-Q. Chu, Q.-Z. Qin, *J. Electrochem. Soc.* **2004**, *151*, A1077.
[24] Y. Sharma, N. Sharma, G. V. S. Rao, B. V. R. Chowdari, *Electrochim. Acta* **2008**, *53*, 2380.
[25] X. Guo, X. Lu, X. Fang, Y. Mao, Z. Wang, L. Chen, X. Xu, H. Yang, Y. Liu, *Electrochem. Commun.* **2010**, *12*, 847.
[26] Y. Deng, Q. Zhang, S. Tang, L. Zhang, S. Deng, Z. Shi, G. Chen, *Chem. Commun.* **2011**, *47*, 6828.
[27] Y. Ding, Y. Yang, H. Shao, *Electrochim. Acta* **2011**, *56*, 9433.
[28] D. Bresser, E. Paillard, R. Kloepsch, S. Krueger, M. Fiedler, R. Schmitz, D. Baither, M. Winter, S. Passerini, *Adv. Energy Mater.* **2013**, *3*, 513.
[29] C. Sotowa, G. Origi, M. Takeuchi, Y. Nishimura, K. Takeuchi, I. Y. Jang, Y. J. Kim, T. Hayashi, Y. A. Kim, M. Endo, M. S. Dresselhaus, *ChemSusChem* **2008**, *1*, 911.
[30] K. Naoi, S. Ishimoto, J. Miyamoto, W. Naoi, *Energy Environ. Sci.* **2012**, *5*, 9363.
[31] J.-H. Kim, J.-S. Kim, Y.-G. Lim, J.-G. Lee, Y.-J. Kim, *J. Power Sources* **2011**, *196*, 10490.
[32] V. Khomenko, E. Raymundo-Piñero, F. Béguin, *J. Power Sources* **2008**, *177*, 643.

